

IR Spectroscopy as a Method for Online Electrolyte State Assessment in RFBs

Oliver Nolte, Robert Geitner, Martin D. Hager, and Ulrich S. Schubert*

The transition from fossil to renewable energy sources requires adequate storage technologies due to the intermittency of the supplied energy. With respect to this, organic redox-flow batteries (ORFBs) represent a promising concept for the storage of electricity on a large scale at economically justifiable costs. However, these storage technologies can only be operated reliably if parameters representing the actual condition of the storage medium (i.e., the electrolyte) can be accurately assessed. These so-called electrolyte state variables are represented by two key figures of merit: state of charge (SOC), a measure of the amount of charge that the electrolyte currently holds; and state of health (SOH), representing the amount of charge that the electrolyte is able to store given its current condition. The herein presented IR-based approach is able to simultaneously provide reliable, fast, accurate, and precise estimates for both SOC and SOH parameters at any point in time and independent of the current battery status. The method is able to provide a time resolution in the range of minutes, is independent of the electrolyte temperature and can be applied to nearly all organic-based redox-active materials and solvents, while potentially being applicable to inorganic RFBs, such as vanadium-based systems, as well.


1. Introduction

Driven by an increased environmental awareness, global energy production will inevitably shift further from the use of fossil and nuclear sources toward renewables. This trend is additionally fueled by decreasing costs for the installation and production of renewable energy, increasing their economic

O. Nolte, Dr. R. Geitner, Dr. M. D. Hager, Prof. U. S. Schubert
Laboratory of Organic and Macromolecular Chemistry (IOMC)
Friedrich Schiller University Jena
Humboldtstr. 10, 07743 Jena, Germany
E-mail: ulrich.schubert@uni-jena.de

O. Nolte, Dr. R. Geitner, Dr. M. D. Hager, Prof. U. S. Schubert
Jena Center for Soft Matter (JCSM)
Friedrich Schiller University Jena
Philosophenweg 7, 07743 Jena, Germany

O. Nolte, Dr. R. Geitner, Dr. M. D. Hager, Prof. U. S. Schubert
Center for Energy and Environmental Chemistry Jena (CEEC Jena)
Friedrich Schiller University Jena
Philosophenweg 7a, 07743 Jena, Germany

 The ORCID identification number(s) for the author(s) of this article can be found under <https://doi.org/10.1002/aenm.202100931>.

© 2021 The Authors. Advanced Energy Materials published by Wiley-VCH GmbH. This is an open access article under the terms of the Creative Commons Attribution-NonCommercial License, which permits use, distribution and reproduction in any medium, provided the original work is properly cited and is not used for commercial purposes.

DOI: 10.1002/aenm.202100931

viability. However, this shift in energy production has a major drawback: While conventional power plants are designed to produce energy on demand with constant output, the intrinsic intermittency of wind, and solar energy productions calls for suitable energy storage solutions, in which redox flow batteries (RFBs) represent a promising solution.^[1] Compared to the current commercially available inorganic systems based on vanadium (VRFB) or zinc–bromine/zinc–iron, the use of organic active materials in RFBs promises a decoupling from commodity prices as well as an environmentally and socially responsible production of the storage materials.^[2] However, organics are prone to decomposition reactions on the molecular level that inevitably occur within the pursued decadal lifetimes required for an economic operation of RFBs.^[3] Thus, methods to accurately assess the key electrolyte state variables

state of charge (SOC) and state of health (SOH) are of paramount importance for these RFB concepts.

As recently reviewed by our group, the most established SOC monitoring methods for RFBs are represented by Coulomb counting (CC) and measurements of the electrolytes' redox potential.^[4] Both methods require either relatively simple measurement equipment (open circuit voltage (OCV) cells) or are implemented into a battery management system (CC) and can therefore be used independently of the RFB chemistry. Nevertheless, both methods are prone to error accumulation and long-term changes and, thus, require frequent recalibration. Furthermore, the CC method can only provide full-cell resolution (i.e., battery state variables) instead of a more informative half-cell resolution, that is able to provide an electrolyte-based state assessment. Apart from the aforementioned methods, spectroscopic methods have as well been used to determine flow battery state variables, in particular for the VRFB, although other chemistries have been investigated as well.^[4,5] Especially UV–vis spectroscopic measurements have been used in this context, due to the relatively simple and reliable setup as well as their ability to provide half-cell resolution. However, due to the nonlinearity of the absorption for optically dense mixtures, as described by the Beer–Lambert law, the hitherto published methods generally rely on empirically-derived calibrations or extremely thin transmittance measurement cells.^[4] Furthermore, UV–vis data of molecular compounds usually bear limited structural information, as the

corresponding molecular orbitals to occupy excited electrons may extend over a large part of the molecule of interest. Apart from this, the use of visible light or even higher frequencies may lead to an increased molecular decomposition when highly reactive organic intermediates are involved. In contrast to this, using the infrared (IR) region of the electromagnetic spectrum has several advantages

- IR light is able to excite molecular vibrations and rotations. With distinct resonances for different moieties within a molecule, the resulting spectra contain a large amount of structural information.
- Compared to other spectroscopic methods, such as NMR or ESR, IR is applicable to a wide range of organic scaffolds and tolerates almost any functional group (e.g., radicals).
- The use of Fourier-transform infrared (FT-IR) techniques is well established and widely used for IR devices, as it enables extremely fast measurement times (down to several tens of milliseconds).
- Contrary to transmittance cells used for UV–vis setups, attenuated total reflectance (ATR) cells allow for the use of highly concentrated solutions, as the penetration depth of the generated evanescent wave is generally in the range of a couple of micrometers (**Figure 1**), enabling a relatively simple measurement cell setup even for measurements at high concentrations.

The use of IR-based methods as a state assessment tool for flow battery electrolytes is comparably rare in the scientific literature. A first report of an IR sensor for a vanadium-based RFB was published by Rudolph et al. in 2013.^[6] In their publication, the authors used an IR LED ($\lambda \approx 950$ nm) as light source and an IR photodiode as detector in a transmittance setup. Due to a strong nonlinear dependency of the attenuation over the applied SOC range, the sensor was calibrated by a combination of OCV and CC approaches a priori. The system produced errors lower than 1%.

As the only other example known to the authors, Duan et al. reported ex situ FT-IR investigations for SOC diagnostics.^[7] Within their study, the authors used an organic nitroxide compound, 2-phenyl-4,4,5,5-tetramethylimidazoline-1-oxyl-3-oxide, for construction of a symmetrical nonaqueous RFB. The SOC determination followed an ex situ approach: After calibration of the FT-IR device in the concentration range of interest, five electrolyte samples were taken out of the battery tanks at different SOCs and investigated offline by IR and ESR. Even though the authors pointed out the applicability of the IR method for in situ SOC diagnostics, no further investigations have been hitherto made.

In our study, we thoroughly investigated the use of IR spectroscopy as an online electrolyte state assessment tool for RFB electrolytes based on organic active materials. Therefore, we applied the well-known *N,N,N*-2,2,6,6-heptamethylpiperidiny

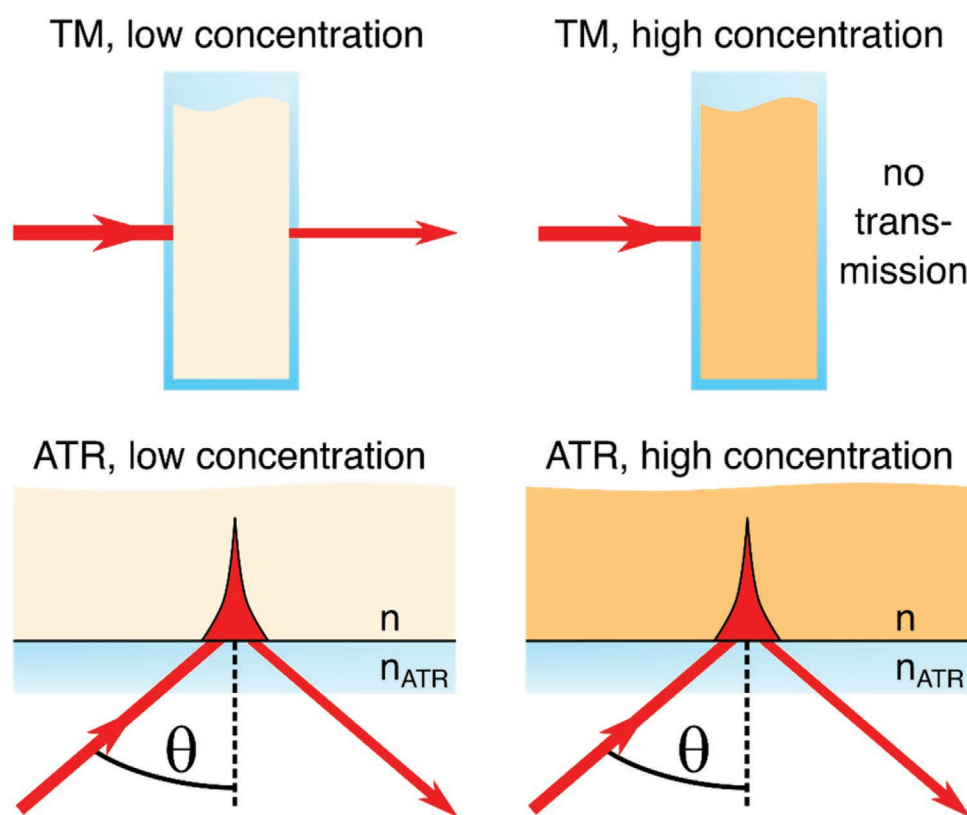


Figure 1. Comparison between transmission and attenuated total reflection (ATR) IR spectroscopy at low and high concentrations. Transmission IR spectroscopy suffers from low transmission rates when the sample is very concentrated as almost all light is absorbed by the sample. This problem is circumvented in ATR-IR spectroscopy by the intrinsic small penetration depth of the evanescent IR light wave.

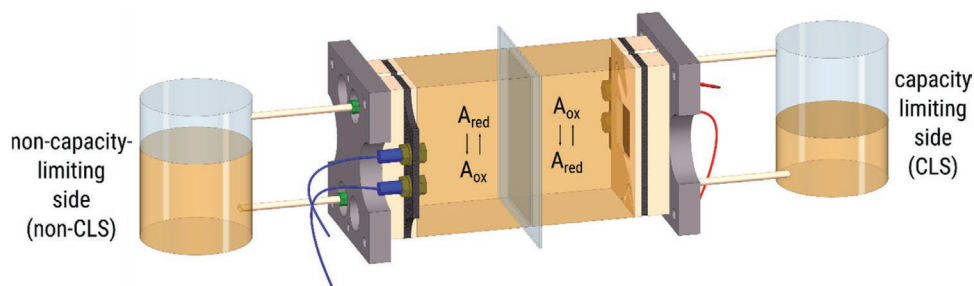


Figure 2. Schematic representation of the unbalanced compositionally-symmetric RFB.

oxy-4-ammonium chloride (TEMPTMA) molecule in an unbalanced compositionally symmetrical flow cell setup, as depicted in **Figure 2** combined with an ATR-FT-IR device and a symmetrical OCV cell.^[8]

2. Results and Discussion

2.1. Data Acquisition and Treatment

As discussed within the introduction, ATR-IR spectroscopy represents a promising tool for the assessment of electrolyte state parameters within RFBs. Nevertheless, during our studies, we encountered some challenges that needed to be overcome before ATR-IR spectroscopy could be used for this purpose: 1) A background correction for the solvent (and supporting electrolyte) used, 2) the influence of water vapor, 3) the wavelength-dependent penetration depth, and 4) temperature changes.

With only a few exceptions, nearly all of the hitherto disclosed RFB chemistries rely on the use of solvents, some further need supporting electrolytes for various reasons. These (mixtures) usually show strong absorbances in the IR region, making a background correction mandatory. In the present case, a background spectrum of pure water has been recorded prior to each measurement series. With this, the majority of the absorption bands of the electrolyte are removed from the consecutive in situ IR measurements. It is not necessary to record a new background during an experiment, as the position and absorbance of liquid water does not change significantly, even if the experiment goes on for multiple weeks. However, especially if highly concentrated solutes are present, the respective absorptions of liquid water may show shifts of their absorption bands, which is often seen for the OH stretching vibration of water above 3000 cm⁻¹.^[9] Using absorption bands of solutes within this region for quantification purposes may thus prove difficult. Fortunately, this effect is less prominent within the fingerprint region of the IR spectrum, and may be addressed by a background correction approach, as done within this study.

Apart from the influence of liquid water, it is commonly known in IR spectroscopy that water vapor can have a significant influence on the quality of the IR spectra, with intense IR absorptions at around 3400, 1600, and 700 cm⁻¹. The IR spectrum of gaseous water features many sharp signals originating from the coupling of rotational and vibrational transitions. Initially, the recorded background spectrum also removes

the signals stemming from water vapor but as the experiment continues, the concentration of water vapor inside the IR beam path changes and, thus, the sharp IR bands of water vapor become visible (see Figure S1, Supporting Information). The best approach to eliminate this unwanted effect is to purge the IR beam path with dry nitrogen or argon, which ideally removes all water vapor from the spectrometer or keeps its concentration at least constant. Unfortunately, this approach is not always feasible, as the utilized IR spectrometer needs to have a gas inlet, which was not the case for the device used in the study at hand. Even though the supplied software has a built-in water vapor compensation tool, the respective bands were not suppressed sufficiently. Luckily, it is also possible to minimize the water vapor bands after the IR spectra have been recorded.^[10] The approach utilized here is based on the fitting of the second derivative of the IR spectrum with the second derivative of the water vapor spectrum (for details see the Supporting Information). This approach takes advantage of the fact that broad peaks disappear in second derivative spectra, while sharp features are preserved. Therefore, the fitting approach is not disturbed by the bands of the sample so long as the peaks are not broad. The resulting fit coefficient can subsequently be used to subtract the water vapor spectrum from the original sample spectrum and, thus, minimize the negative effect of water vapor on the recorded IR spectra. However, as the influence of water vapor cannot entirely be suppressed using this method, both the precision and accuracy of the derived SOC and SOH values may be compromised when using bands overlapped by water vapor features.

After the influence of water vapor is minimized, the IR spectra need to be corrected for the varying light penetration depth in the ATR configuration. Light of smaller wavenumbers/longer wavelengths penetrates deeper into the sample than light of larger wavenumbers/shorter wavelengths, according to the following equation (see Figure S2, Supporting Information)^[11]

$$d = \frac{\lambda}{2\pi \cdot n_{\text{ATR}} \sqrt{\sin^2(\theta) - (n/n_{\text{ATR}})^2}} \quad (1)$$

where d [m] is the penetration depth (which is equivalent to the optical path length in transmission IR spectroscopy), λ [m] is the wavelength, n_{ATR} is the refractive index of the ATR crystal, n is the refractive index of the sample, and θ [°] is the incident angle of the IR light. Therefore, it is necessary to correct for the varying penetration depth to avoid the overestimation of absorbances at smaller wavenumbers, as this would otherwise

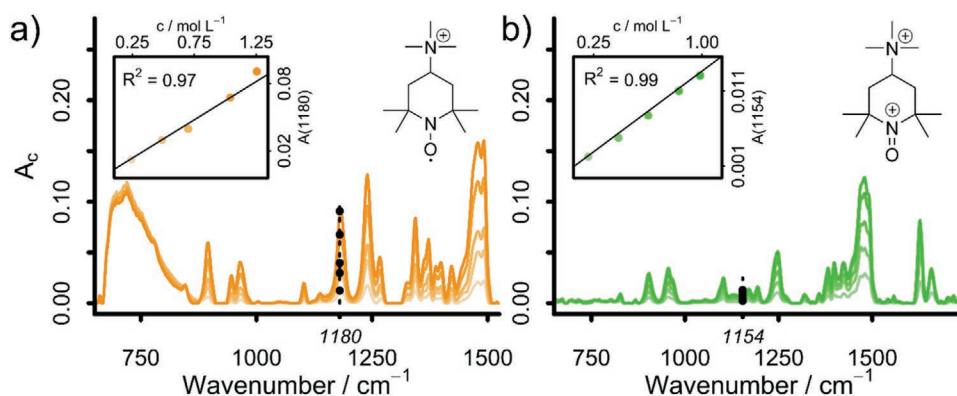


Figure 3. Baseline and ATR-corrected IR spectra of TEMPTMA (a, left panel, orange) and TEMPTMA⁺ solutions (b, right panel, green) with varying concentrations. The inset shows the absorbances at 1180 (TEMPTMA) and 1154 cm^{-1} (TEMPTMA⁺) plotted against concentration. As can be seen, the absorbance is linearly dependent on the concentration. This fact allows for the use of the Beer–Lambert law. Counter ions have been omitted. The color scale is indicative of the respective concentration, with more saturated colors implying higher concentrated solutions.

skew the following SOH analysis. Thus, it is important to know the penetration depth as it is used to correct the recorded ATR-IR spectra. The correction is based on the Beer–Lambert law which describes a linear relationship between absorbance A and penetration depth d [m]

$$A = c \cdot \varepsilon \cdot d \quad (2)$$

using the sample concentration c [mol L^{-1}] and the wavenumber-dependent extinction coefficient ε [$\text{L m}^{-1} \text{mol}^{-1}$]. By dividing A by d , a corrected absorbance, A_c , can be calculated which is independent of d

$$A_c = \frac{A}{d} = c \cdot \varepsilon \quad (3)$$

This corrected absorbance can subsequently be used to first calculate ε from a series of calibration measurements and then to estimate an unknown c when ε and the species within the sample are known.

Finally, a baseline correction is necessary to account for the influence of temperature changes during the in situ IR measurements. As can be seen from Figure S3 (Supporting Information), the recorded IR absorbance shows a strong dependence even on small variations in temperature. A systematic study revealed that this effect is based on an increasing offset added to all wavenumber positions which stems from the difference in measurement temperature between background and sample spectrum. This offset can become much larger than the changes stemming from the varying concentrations during the battery charging and discharging process. In ex situ IR spectroscopy, it is thus best practice to always record a fresh background spectrum for each new sample. This approach is not possible for in situ measurements, as the sample is constantly in contact with the ATR crystal and, thus, it is not possible to record a fresh background spectrum during the measurement. Luckily, an offset can be easily removed with a baseline correction, (for details see the Supporting Information) which in turn also removes the influence of varying temperatures on the IR measurements (see Figure S3, Supporting Information).

2.2. Concentration Dependency

With all known technical difficulties resolved, the first step toward the implementation of IR spectroscopy as an online monitoring tool for organic RFBs was to choose a suitable model system. We decided to use the well-known TEMPO-based TEMPTMA system, as it represents a promising polysolite material for ORFBs.^[12] TEMPTMA features a single electron oxidation to form TEMPTMA⁺, an *N*-oxoammonium cation. It furthermore is insensitive toward atmospheric oxygen and produces binary mixtures at intermediate SOC values.

Figure 3 depicts the IR spectra of TEMPTMA and TEMPTMA⁺ at different concentrations. As can be expected, both molecules feature some distinct absorbances in their vibrational spectrum. The most important band of TEMPTMA⁺ is the N=O stretching vibration at 1626 cm^{-1} , which cannot be found in TEMPTMA.^[13] Apart from that, both IR spectra are fairly similar with C–H deformation vibrations at 1480 cm^{-1} or C–C vibrations at 1230 cm^{-1} . Besides qualitative information in the band position, IR spectra also contain quantitative information in the form of extinction coefficients. Equation (3) shows how the extinction coefficient ε can be calculated from the corrected absorbance A_c if the concentration is known. Exemplarily, the insets in Figure 3 display the absorbance at 1180 and 1154 cm^{-1} plotted against the TEMPTMA and TEMPTMA⁺ concentration, respectively. As the Beer–Lambert law predicts, the relation between absorbance and concentration is linear, even at high concentrations which are commonly found in RFBs (see Figures S5 and S6 as well, Supporting Information). This is the major advantage of ATR-IR spectroscopy compared to transmission IR spectroscopy as even concentrations >1 M can be quantitatively analyzed. From the recorded concentration dependent IR spectra, the extinction coefficients ε for all wavenumber positions can be calculated. ε for the most important bands of TEMPTMA and TEMPTMA⁺ are summarized in Tables S3 and S4 (Supporting Information), respectively. These coefficients are crucial, as they enable the calculation of the concentration of a known sample from its IR absorbance according to Equation (3).

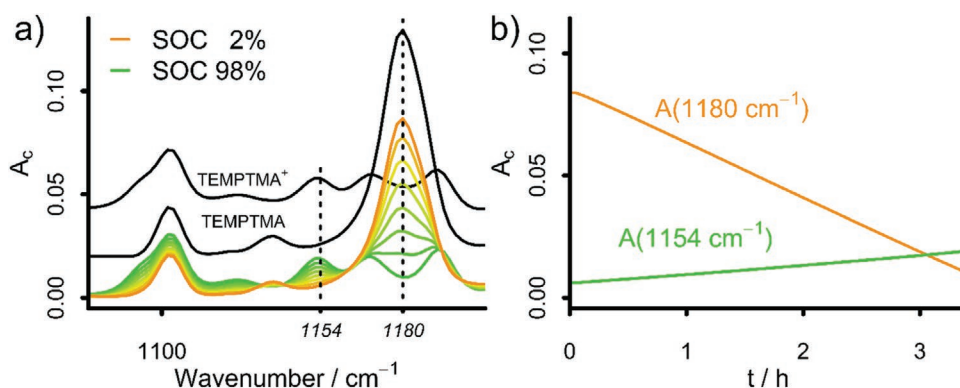


Figure 4. a) Selected baseline and ATR corrected IR spectra recorded in situ during the galvanostatic charging of an unbalanced compositionally-symmetric TEMPTMA/TEMPTMA⁺ RFB. For reference, the IR spectra of an aqueous TEMPTMA and TEMPTMA⁺ solution are also shown. b) IR absorbances at 1154 and 1180 cm⁻¹ during galvanostatic charging.

Additionally, it is noteworthy to say that IR spectroscopy is a powerful technique that is able to simultaneously provide quantitative information about the concentration of all IR active species, as well as a vibrational fingerprint, which can be used to identify different components of the analyzed mixture. As both redox-active and inactive, molecules can be investigated, IR spectroscopy may be especially useful to provide information about electrochemically silent compounds of the mixture, e.g., supporting electrolytes or unknown degradation products. However, in these cases the complexity of the mixture may prove to be a special challenge. Thus, the use of more complex regression models and spectral deconvolution approaches may be beneficial.

While the presented case study will strongly focus on the determination of the operationally important SOC and SOH parameters in a binary electrolyte system, the scope of this IR spectro-electrochemical approach promises to provide a tool to further qualify and quantify crossover and decay processes in RFBs, which will be within the focus of subsequent studies.

2.3. SOC Detection

With the molar extinction coefficients of TEMPTMA and TEMPTMA⁺ at hand, it is possible to deduce the molar fraction of either component within the binary mixture. The molar fraction of the charged species—TEMPTMA⁺ in the present case, χ_{ox} —is equivalent to the electrolyte state of charge (SOC_E) of the associated half-cell in a RFB. This is formalized in the following equation

$$\text{SOC}_E = \frac{c_{\text{ox}}}{c_{\text{red}} + c_{\text{ox}}} = \frac{n_{\text{ox}}/V}{n_{\text{red}}/V + n_{\text{ox}}/V} = \frac{n_{\text{ox}}}{n_{\text{red}} + n_{\text{ox}}} = x_{\text{ox}} \quad (4)$$

where c_{red} and c_{ox} [mol L⁻¹] are the concentrations, n_{red} and n_{ox} the amounts of the uncharged and charged species (here, TEMPTMA and TEMPTMA⁺) and V [L] is the respective electrolyte volume. As c_{red} and c_{ox} are both available from a single IR measurement according to Equation (3), an SOC_E value can be determined from a single IR spectrum. For this analysis c_{red} and c_{ox} need to be calculated from the IR absorbance of the binary mixture using the previously extracted extinction coefficients of the pure components. In principle, each wavenumber

position can be used for this calculation but the accuracy of the SOC determination increases when wavenumber positions are chosen that show strongly differing extinction coefficients for the respective TEMPTMA and TEMPTMA⁺ species. In this study, we chose to use 1180 and 1154 cm⁻¹, which fulfilled these criteria.

Following the band selection process, in situ experiments using an unbalanced compositionally symmetric cell setup were conducted. With this setup, the SOC of the electrolyte used in the capacity limiting half-cell can be fully varied within the majority of the SOC range (as the ideal extremum values of zero and one cannot be attained). **Figure 4a** depicts the selected in situ IR spectra, which were recorded during the galvanostatic charging of the RFB cell for both wavenumbers, starting at a low SOC. The IR spectra nicely show the decreasing concentration of TEMPTMA and simultaneous increase of the concentration of its respective oxoammonium cation, with the IR spectra increasingly resembling a fully charged electrolyte. This qualitative observation is quantitatively shown in **Figure 4b**, where the absorbances at 1154 and 1180 cm⁻¹ are plotted against time. Both figures furthermore demonstrate the binary nature of the used redox couple: While **Figure 4a** shows several isosbestic points, **Figure 4b** displays a linear dependency of the absorbance of both wavenumbers against time within the galvanostatic charging regime. As discussed, these absorbances can be converted into the respective concentrations of TEMPTMA and TEMPTMA⁺ according to Equation (3), from which the SOC_E of the capacity-limiting half-cell can be calculated using Equation (4). As expected from Faraday's Law, the SOC of the electrolyte changes linearly during the galvanostatic charging process ($I = \text{const}$). In order to prove the validity of the IR spectroscopic SOC measurement, the IR derived SOC_E values were compared to the SOC values calculated by a measurement of the electrolyte's redox potential during each galvanostatic half-cycle using a symmetrical OCV cell.^[8] The resulting E/t -curve represents a sufficiently large part of the SOC range and can be fitted according to the Nernst equation (see **Figure 5a**), as reported by Ressel and Stolze,^[8,14] using a three parameter fit to extract E_{ref} , t_0 , and t_{tot} with the following equation (valid for $I = \text{const}$).

$$E = E_{\text{ref}} \pm \frac{RT}{nF} \ln \left(\frac{t + t_0}{t_{\text{tot}} - t - t_0} \right) \quad (5)$$

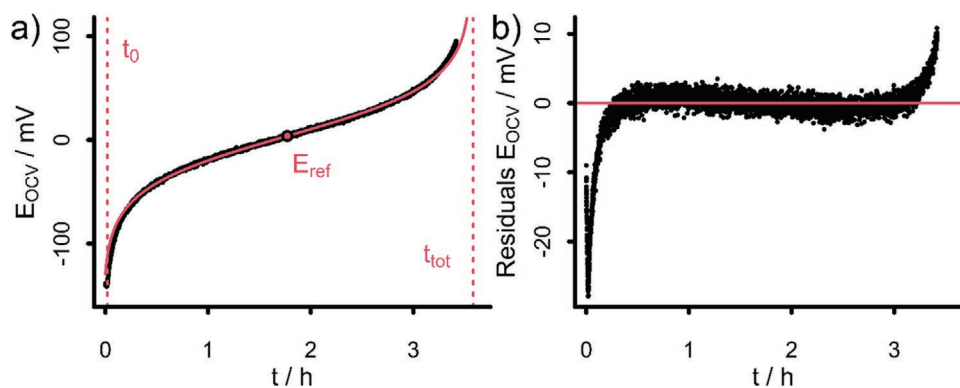


Figure 5. a) Potential recorded by a symmetric OCV cell during the same galvanostatic charging process as shown in Figure 4. The curve can be fitted by the Nernst equation to extract t_0 , t_{tot} , and E_{ref} (shown in red). b) Residuals of the fitting process shown in a). The fit shows higher deviations at the start and at the end of the charging process.

where E [V] represents the measured OCV potential, E_{ref} [V] is the reference potential of the reference electrolyte, R [$J \text{ mol}^{-1} \text{ K}^{-1}$] is the gas constant, T [K] is the absolute temperature, n is the number of electrons transferred, F [$A \text{ s mol}^{-1}$] is the Faraday constant, and t [s] is the time, while t_0 and t_{tot} represent the theoretical time extrema for fully discharged and fully charged electrolytes, respectively. The sign of the concentration dependent logarithmic term is positive for polysolutes and negative for negolytes.

Subsequently, the SOC_E is calculated according to

$$SOC_E = \frac{1}{1 + e^{\frac{-nF}{RT}(E - E_{ref})}} \quad (6)$$

Figure 6a displays a comparison of the SOC_E values obtained during the reference time period, showing good agreements with the expected linear SOC-time dependency for both methods within the galvanostatic charging segment.

However, as demonstrated by plotting the fit residuals (Figure 5b), the redox potential recorded by the OCV cell deviates from the ideal fit, resulting in a deviation from ideal linearity in Figure 6a. These deviations are intrinsic for measurements of the redox potential of a solution, and stem from several sources: 1) The potential of the reference half-cell has to be stable within

the half-cycle (crossover and molecular decomposition have to be excluded), 2) the solution temperature has to remain constant over the course of the half-cycle, 3) a sufficient (ideally infinite) timeframe has to be applied to measure equilibrium potentials, 4) the activity coefficients are generally assumed to be unity for the redox species of interest and the corresponding ions participating in the redox reaction, using concentrations in lieu thereof,^[15] 5) the redox potential of the measurement half-cell is sensitive to all electrochemically active species, which also includes impurities (e.g., foreign metal ions), solvent ions (e.g., hydrogen and hydroxy ions) or dissolved gasses (e.g., oxygen),^[15,16] and 6) the applied SOC change is assumed to be ideally linear with respect to time (or charge) (i.e., exactly constant (or known) current, no side-reactions, purely faradaic currents). Furthermore, frequent recalibrations have to be performed, as the reference potential is generally not stable over an extended period of operation (several cycles). Nevertheless, the general ease-of-use of redox potential measurements, their negligible hardware costs and applicability to a wide range of redox couples, combined with the production of reliable SOC estimates renders this method a standard electrolyte SOC assessment tool.

Spectroscopic methods, such as the presented technique using an ATR-IR spectroscopic cell, on the other hand, suffer from deviations from the theoretically linear relationship of

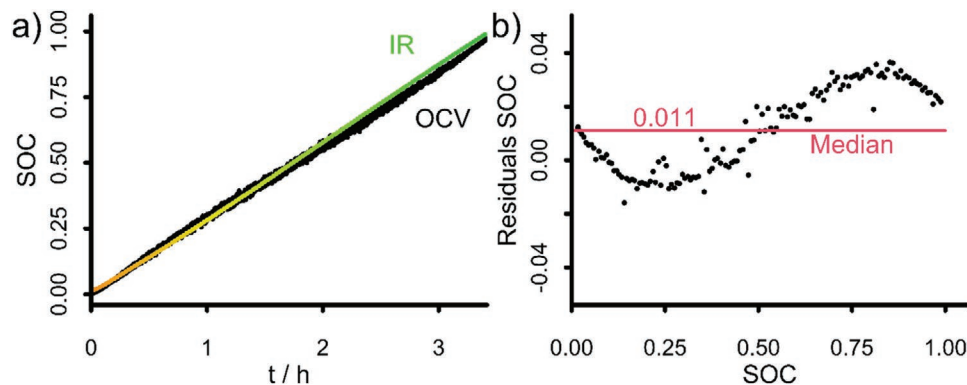


Figure 6. a) SOC calculated from the IR spectra (orange-green line) and from the OCV potential (black line), recorded for the RFB charging process shown in Figure 4. As expected, both curves are highly linear during the galvanostatic charging process. b) Difference of the two SOC curves shown in a). The median deviation between IR and OCV determined SOC is 1.1 %. Figure S8 shows these data recorded over an increased timeframe of several cycles as well as the absolute values of the residuals.

concentration and absorption described by the Beer–Lambert law: 1) The high concentrations of the redox-active materials and supporting electrolytes as well as the composition changes induced by the variation of the SOC within the electrolyte used in RFBs facilitates the development of electrostatic interactions between the solution species, leading to a change in ϵ , 2) ϵ at a specific wavenumber must be known for the species of interest, meaning that either only one species absorbs light at a given wavenumber or that the contribution of other species must also be known, 3) the optical path length (d , see Equation (3)) has to remain constant (we are using an ATR correction within this publication), and 4) scattering effects have to be minimized or should at least be wavelength-independent.

Furthermore, ϵ usually has to be determined for the wavelength and species of interest (done with a calibration), before a spectroscopic method can be used for the determination of concentrations. Apart from this, changes in the electrolyte temperature have to be accounted for as well. This can be done by a calibration or, as discussed, with a baseline correction approach.

Compared to a linear fit of the recorded data, the SOC precision shows a median deviation of 0.024% with a standard deviation of 0.43%. Furthermore, comparing both the OCV and the IR methods, we found the median difference of the SOC_E estimates to be around 1% with a standard deviation of 1.88% (see Figure 6b; and Figure S9, Supporting Information). Thus, it can be concluded that in situ IR spectroscopy is a precise and accurate tool comparable to OCV cells to monitor the SOC_E of a RFB.

2.4. SOH Detection

Apart from the SOC, the SOH represents another important parameter for the state assessment of a RFB. The SOH defines the ratio of the theoretically accessible amount of charge of a battery at a selected point in time with respect to a reference value, usually defined at $t = 0$. As for the SOC, the SOH can be expressed for both the battery (SOH_B) as well as the distinct half-cell electrolytes (SOH_E). Omitting activity coefficients and concentration gradients within the electrolyte, the SOH_E can thus be expressed by the ratio of the total concentration of the redox-active species, c_{tot} , and the total concentration of the redox-active species at a reference time, $c_{\text{tot,ref}}$, usually given at the initial start-up of the battery. In the binary TEMPTMA/TEMPTMA⁺ system, c_{tot} can be calculated from the concentrations of the two individual species c_{red} and c_{ox} . This is expressed by the following equation

$$\text{SOH}_E = \frac{c_{\text{tot}}}{c_{\text{tot,ref}}} = \frac{c_{\text{ox}} + c_{\text{red}}}{c_{\text{ox,ref}} + c_{\text{red,ref}}} \quad (7)$$

As was the case for the SOC determination, c_{ox} and c_{red} can be extracted from a single IR measurement according to Equation (3), if the extinction coefficients ϵ are known. In the same manner, $c_{\text{ox,ref}}$ and $c_{\text{red,ref}}$ can be obtained. Thus, the SOH can be determined from two distinct IR measurements according to Equation (7): One spectrum needs to be taken at the reference point while the other one probes the system at the time of interest. Interestingly, this is independent of the current SOC of the electrolyte, enabling a SOH detection at any point in time.

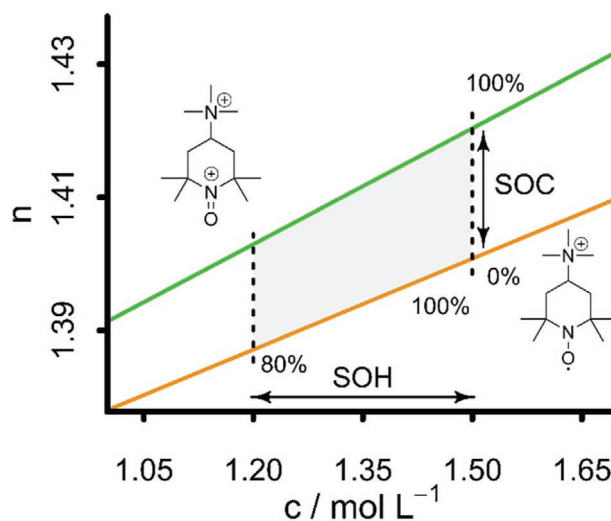


Figure 7. Concentration-dependent refractive indices of TEMPTMA (orange line) and TEMPTMA⁺ (green line), see Figure S5 and S6 as well. The refractive index changes with the SOC as well as the total electrolyte concentration (SOH), respectively. The grey area marks the relevant refractive indices for a RFB that is cycled between 0% and 100% SOC within the SOH range of 100 to 80%.

Although the SOH analysis seems to be identical to the SOC determination, the procedure is not straightforward. The challenge that arises when comparing two IR spectra taken at arbitrary SOC values is the change in refractive index when the composition of the probed solution changes (see Figure 7). To account for this change in refractive index, we developed an advanced correction approach: First, the refractive indices at different concentrations of aqueous TEMPTMA and TEMPTMA⁺ solutions were measured (see Tables S1 and S2, Supporting Information, respectively). Second, an arbitrary ATR correction was performed according to Equation (1) using one refractive index for all IR spectra independent of the SOC. Subsequently, the SOC was determined from each IR spectrum. The SOC is independent of the refractive index according to Equation (4), as both the numerator and the denominator are dependent in the same way on the light penetration depth and, consequently, the refractive index. As long as an ATR correction is applied, it does not matter for the SOC determination which sample refractive index was used for the correction procedure. The SOC is then used to estimate the volumetric fraction φ_1 and φ_2 of the TEMPTMA and TEMPTMA⁺ phases of the solution. For instance, an SOC of 50% denotes that 50% of the volume of the electrolyte solution is made up of an aqueous TEMPTMA solution while the remaining 50% is made up from an aqueous TEMPTMA⁺ solution. These volumetric fractions are then used together with the previously determined refractive indices of the pure solutions to calculate the refractive index of the mixture according to the Lorentz–Lorenz equation^[17]

$$\frac{n_M^2 - 1}{n_M^2 + 2} = \varphi_1 \frac{n_{\text{red}}^2 - 1}{n_{\text{red}}^2 + 2} + \varphi_2 \frac{n_{\text{ox}}^2 - 1}{n_{\text{ox}}^2 + 2} = (1 - \text{SOC}) \cdot \frac{n_{\text{red}}^2 - 1}{n_{\text{red}}^2 + 2} + \text{SOC} \cdot \frac{n_{\text{ox}}^2 - 1}{n_{\text{ox}}^2 + 2} \quad (8)$$

where n_{red} , n_{ox} , and n_M are the refractive indices of an aqueous TEMPTMA, an aqueous TEMPTMA⁺ solution and

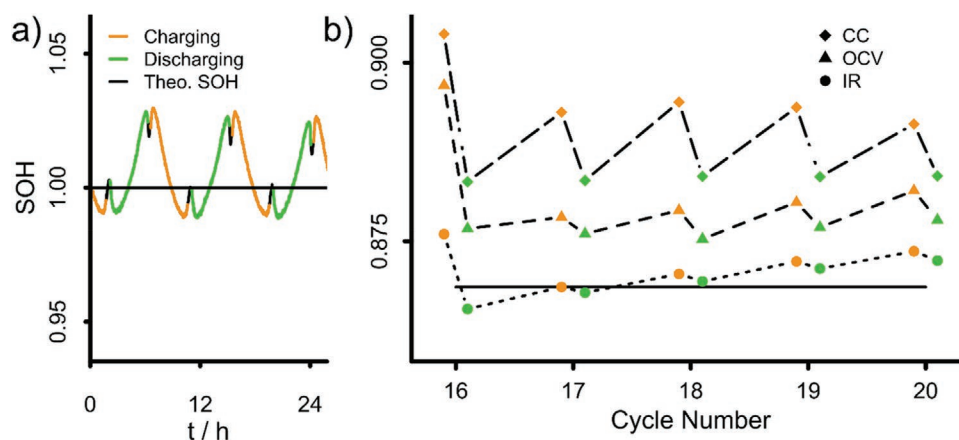


Figure 8. a) SOH calculated by IR spectroscopy. The first spectrum recorded is used as reference. The precision of the technique is around 3% within one half-cycle when compared to the theoretical SOH. b) Comparison of different SOH determination techniques during multiple charging/discharging cycles with constant SOH. CC (diamonds), OCV half cycle fitting (triangles) and IR spectroscopy (circles) are compared to the theoretically expected SOH (black line). Orange lines/symbols denote data collected during battery charging while green lines/symbols denote data collected during battery discharging.

TEMPMA/TEMPMA⁺ mixture. n_{red} and n_{ox} can be estimated from the recorded data points for any total concentration as both scale linearly with the concentration (see Figures S5 and S6, Supporting Information). n_{M} is then used to perform the proper ATR correction for each spectrum. The SOC_E remains unchanged from this procedure, while the accuracy of the SOH_E determination is improved by the use of the correct refractive index.

Although this procedure helps to improve the mutual accuracy of the SOH_E estimates, it also has two sources of error: The first one is the total electrolyte concentration used to calculate the refractive indices of the pure solutions. As indicated in Figure 7, the refractive index range accessed by the variation of the SOC_E is shifting with any variation of the total concentration of the redox-active species within the electrolyte, and thus with variations in SOH_E . The presented correction approach cannot account for this change in total concentration and, thus, leads to a systematic error. This error is larger if the change in total concentration is larger. If one performs the correction procedure assuming a total electrolyte concentration of 1.5 M, although in reality the concentration is just 1.2 M (corresponding to an SOH of 80%), the SOH_E determination is off by around 0.9% at SOC_E values of 0% and 100%. A second source of error is the assumption that the SOC_E can be directly related to the volumetric fraction of the TEMPMA⁺ phase. As Equation (4) reveals, the electrolyte SOC is equivalent to the molar fraction of TEMPMA⁺, not to the volumetric fraction. This is only the case if the densities of the aqueous TEMPMA and TEMPMA⁺ solutions are identical, and no secondary effects occur, which further alter the density of the mixture. As intended by the addition of a sodium chloride solution instead of pure water in the following experiment, the expected change of the refractive index of the mixture should be smaller than indicated in Figure 7, as density and refractive index of the used 1.5 M sodium chloride solution ($\rho = 1.0604 \text{ g mL}^{-1}$, $n = 1.3485$) are similar to the used electrolytes. This may as well be the case for a commercially used RFB electrolyte, in which crossover species or decomposition products of the redox-active molecules

indeed alter the SOH_E but may not represent the changes in density and refractive indices induced by a mutual dilution with pure solvents. Thus, the impact on the SOH determination by the two assumptions is considered minimal and well below the deviation that would be introduced, if the same refractive index were to be assumed for all charging states.

In order to validate the proposed SOH measurement method, an approach to artificially change the SOH_E of the monitored half-cell was utilized. This approach was chosen to induce SOH changes independent of crossover and decomposition-related concentration changes. For this purpose, the concentration was reduced by removing aliquots of the TEMPMA/TEMPMA⁺ solution and replacing them with an equal volume of sodium chloride solution until a theoretical SOH of less than 80% was achieved. Figure 8a depicts the IR derived SOH_E estimates at arbitrary SOC_E values over the course of a full cycle for a (theoretically) constant SOH_E . It is clearly visible that the SOH varies by about 3% within a cycle. This deviation from the theoretically expected SOH correlates with the SOC of the electrolyte. It is not quite clear what is causing this variation, but it seems to be linked to the Beer–Lambert law and the utilized extinction coefficient. We hypothesize that there is some kind of weak molecular interaction between TEMPMA and TEMPMA⁺ or an optical dispersion effect, which slightly alters their extinction coefficients. Obviously, this interaction will scale with the concentration of both molecules in solution. Nevertheless, the achieved precision of around 3% for an SOH_E determination at arbitrary SOC values and purely based on the Beer–Lambert law is remarkable. It is easy to further improve this accuracy if more advanced models based, e.g., on regression analysis^[18] or neural networks^[19] are applied.

As mentioned before, the Nernst fit of the OCV cell data (see Equation (5) as well as Figure 4c) produces several fitting parameters, of which t_{tot} can be used to monitor the SOH_E of a RFB.^[8,14] However, in order to produce this fitting parameter, a sufficiently large portion of the potential-time (or potential-charge) curve needs to be recorded, with an increasing accuracy of the estimate for larger parts of the respective curve. Per

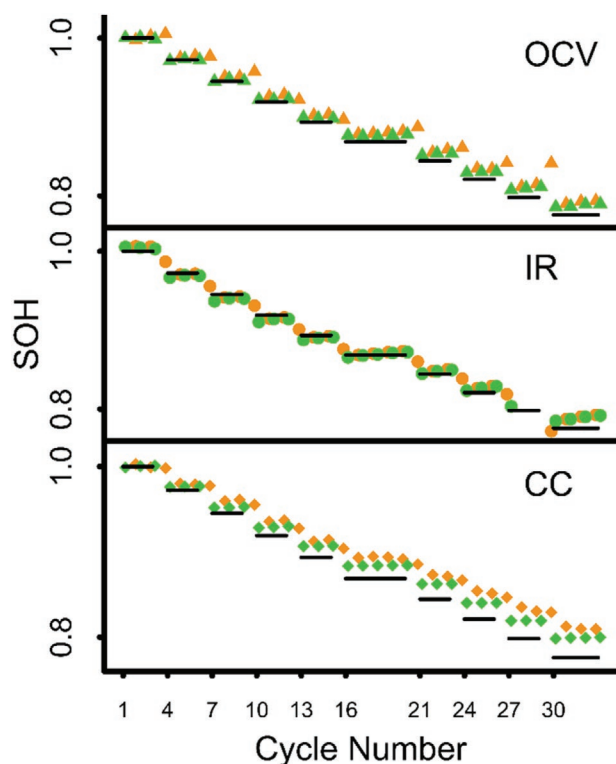


Figure 9. Comparison of different SOH determination techniques. CC (diamonds), OCV half cycle fitting (triangles) and IR spectroscopy (circles) are compared to the theoretically expected drop off (black lines) during the artificially induced SOH changes. The total duration of the experiment was 266 hours. Orange lines/symbols denote data collected during battery charging while green lines/symbols denote data collected during battery discharging.

half-cycle, this parameter can only be assessed once. Figures 8b and **Figure 9** compare the SOH_E estimates derived by the IR and OCV methods and indicate the SOH_B values derived by CC as well as the theoretically expected SOH_E values. The IR derived SOH_E estimates shown are averaged over one half-cycle for clarity reasons. Both OCV and IR techniques are able to detect the artificially induced SOH changes. However, the presented IR method reveals the smallest discrepancies from the theoretically expected SOH values with a calculated median deviation of 0.16% (and a standard deviation of 1.28%). As shown in Figure S9 (Supporting Information), the deviation of both OCV and IR methods is relatively small, with a median deviation of 0.7% and a standard deviation of 1.07%.

A closer look at the presented data in Figure 8b shows increasing SOH estimates over several cycles within a cycling segment with constant theoretical SOH (black lines) for all methods. This trend is visible for both the OCV and IR derived values. Our interpretation of this observation is that crossover between the half-cells of the symmetric TEMPTMA/TEMPTMA⁺ RFB increases if the concentration in the monitored, capacity limiting half-cell, drops. This is to be expected as the increasing difference in electrolyte concentration will lead to an increased diffusion of electrolyte molecules across the RFB membrane. Furthermore, as the entire monitoring equipment (OCV cell and IR device) is situated in the fluid circuit of

one half cell, a significant pressure gradient between the half-cells can be expected, which is leading to an increase in crossover related SOH changes. As lower theoretical SOH values are realized at longer experiment times, the cumulated impact of crossover is higher at later stages of the experiment.

Furthermore, Figure 8b reveals an influence of the direction of SOC change for the SOH estimates of all techniques, with higher estimates produced during the charging half-cycle. This deviation is highest for the CC approach, in which this is usually designated as the Coulomb efficiency. While the OCV cell, due to its (not entirely independent) fitting approach, produces smaller discrepancies, these are comparably small for the presented IR method. However, for the IR method, it is still not entirely clear to us where these stem from, as this effect does not seem to originate from the same sources as the deviations depicted in Figure 8a. A possible explanation could be based on the different crossover rates of the redox-active species, which would lead to deviations of the net crossover depending on the direction of current flow, similar to investigations conducted for vanadium-based electrolytes.^[20]

At this point, we want to stress that in particular the SOH_E estimates produced by the OCV cell are not fully independent of the CC approach. Thus, any comparison of the SOH_B estimates obtained by the CC approach and SOH_E estimates produced using the OCV cell data has to be treated with caution. Furthermore, the SOH_B estimates derived by the CC approach and SOH_E estimates usually cannot be compared, unless the respective half-cell electrolytes are perfectly balanced or other measures to assess the true amount of charge related to the total concentrations of the redox-active materials are introduced. Additionally, the applied charge has to entirely drive faradaic charge transfer processes of the redox-active species, which is usually not the case. In our experiments, we tried to enforce this with the utilization of the unbalanced compositionally symmetric cell cycling method in combination with potentiostatic cycling near the extremum SOCs, in which the transferred amount of charge is largely defined by the capacity of the capacity-limiting half-cell.

Even though the same setup was used to produce solutions of TEMPTMA⁺ for the definition of $SOC_{E,max}$, the recorded IR spectra can be regarded to be independent of the charging time (or the transferred amount of charge) and, thus, independent of the CC approach. The spectra used to define the extremum SOC values are therefore only reliant on the purity of the respective substances. It can be concluded that in situ IR spectroscopy, coupled with a suitable evaluation approach, is a reliable tool to monitor the SOH_E in ORFBs.

3. Conclusion

In this work, we presented a new in situ electrolyte assessment method for the fast, reliable, and precise assessment of the key electrolyte state parameters SOC_E and SOH_E based on an FT-IR device equipped with an ATR flow cell, enabling a measurement even at high analyte concentrations, as encountered in flow battery electrolytes. The proposed IR method is expected to be transferrable to a wide range of different RFB chemistries based on organics and applicable to nearly all solvents. With

the presented experiments, we investigated the applicability of the presented method and assessed its precision by comparison with the data obtained from a symmetrical OCV cell. For our experiments, we exemplarily used aqueous electrolytes containing the well-investigated aminoxyl radical TEMPTMA in an unbalanced compositionally symmetrical RFB.

In the first part of this publication, we presented methods to account for common interferences and physical peculiarities of the used setup: The influence of humidity, temperature, and the wavelength-dependency of the IR penetration depth. The presented approaches are easily reproducible and are transferable to other devices, even though other approaches to eliminate these influences may be applicable as well (e.g., flushing the beam path with dry nitrogen to eliminate water vapor).

Within the core parts of the presented work, we investigated the use of the presented method to assess the SOC_E and SOH_E parameters of the organic electrolyte. For this, the following requirements have to be fulfilled

- The extinction coefficients for all IR-active species at the wavelengths of interest have to be known;
- a spectrum of the solution containing only the pure species present at each SOC extrema has to be recorded;
- the refractive indices of the solution containing only the pure species have to be known for the concentration (range) of interest (only needed for SOH determination).

Even though a number of assumptions were made, the presented method achieves a remarkable accuracy, with errors of around 2% and 1% for the SOC_E and SOH_E estimation, respectively, when compared to the readout of the OCV cell, while the precision of the method is around 0.02% for the SOC_E estimation and 0.2% for the SOH_E estimation. Furthermore, once running, the method is able to deliver SOH_E estimates at any point of interest by comparison of two spectra regardless of the current SOC_E , which, to the best of our knowledge, has not been shown before with the accuracy and precision mentioned above.

Additionally, apart from the herein presented state assessment tool, the presented setup may be further interesting for the investigations of crossover and decomposition related electrolyte changes, as the structural information present in the spectra can be used as well. Furthermore, the method's applicability to other organic redox-active materials representing more complex mixtures than the binary system used within this study has to be investigated. This is subject to ongoing investigations.

4. Experimental Section

The used solutions of TEMPTMA and methyl viologen (MV) were supplied by JenaBatteries GmbH, Germany.

All battery experiments as well as data acquisition for the OCV cell were conducted using a VMP-3 potentiostat/galvanostat (Bio-Logic, France). The used RFB cells were custom-made flat-type cells using graphite current collectors, GFA-6 felts (SGL, Germany) and FAA-3-50 anion exchange membranes (fumatech GmbH, Germany) with an effective membrane area of 5 cm². As OCV cell, a custom-made two-compartment electrochemical cell using an FAA-3-50 membrane and graphite electrodes was employed. Electrolyte solutions used within the unbalanced compositionally symmetric cell setup were prepared by charging a TEMPTMA/MV cell with a slightly oversized (110%)

MV half-cell to full capacity (potentiostatic cycling with a voltage limit of 1.45 V and a current limit of 1 mA cm⁻² at high SOC) and mixing of the generated solution containing the TEMPTMA oxoammonium cation with an equal amount of uncharged TEMPTMA solution in order to generate a solution of 50% SOC. This electrolyte composition was used as reference electrolyte for the OCV cell as well. Symmetric cell experiments were conducted with a driving voltage of 0.45 V in either direction and potentiostatic cycling at the SOC extrema with a current limit of 5 mA (1 mA cm⁻²).

In situ infrared (IR) spectra were recorded using a liquid nitrogen-cooled ReactIR 701L (Mettler Toledo, Germany), equipped with a Micro Flow Cell DS DiComp (Mettler Toledo, Germany) between 650 and 4000 cm⁻¹ at a resolution of 4 cm⁻¹ using a diamond ATR crystal. A background spectrum of deionized water was collected with 128 single scans prior to each experiment. Each individual in situ IR spectrum consists of 138 single scans, which corresponds to a measurement time of 90 s per spectrum. The same number of scans was used during the TEMPTMA and TEMPTMA⁺ concentration calibration measurements and to collect a series of water vapor spectra.

The implementation of both measurement methods (OCV and IR) within the experimental setup is depicted in Figure S10 (Supporting Information).

Supporting Information

Supporting Information is available from the Wiley Online Library or from the author.

Acknowledgements

O.N. and R.G. contributed equally to this work. The authors kindly thank the Thüringer Aufbaubank (TAB) and the Thuringian Ministry of Economic Affairs, Science and Digital Society (TMWdG) for financial support. The study was co-financed by the state of Thuringia (No. CEEC-01/2020). The project on which these results are based was funded by the Free State of Thuringia under the No. 2016 IZN 0009 and cofinanced by funds from the European Union within the framework of the European Regional Development Fund (ERDF). The Federal Ministry for Economic Affairs and Energy (BMWi) is acknowledged for financial support within the project PhotoFlow. The authors furthermore thank JenaBatteries GmbH for providing the TEMPTMA and MV electrolyte stock solutions.

Open access funding enabled and organized by Projekt DEAL.

Conflict of Interest

The authors declare no conflict of interest.

Data Availability Statement

The data that supports the findings of this study are available in the supplementary material of this article.

Keywords

electrolyte state assessment, IR spectroscopy, online monitoring, redox-flow battery, SOC and SOH determination

Received: March 21, 2021

Revised: May 11, 2021

Published online: June 9, 2021

- [1] a) M. S. Ziegler, J. M. Mueller, G. D. Pereira, J. Song, M. Ferrara, Y.-M. Chiang, J. E. Trancik, *Joule* **2019**, *3*, 2134; b) O. Schmidt, S. Melchior, A. Hawkes, I. Staffell, *Joule* **2019**, *3*, 81; c) T. M. Gür, *Energy Environ. Sci.* **2018**, *11*, 2696.
- [2] R. R. Moskalyk, A. M. Alfantazi, *Miner. Eng.* **2003**, *16*, 793.
- [3] a) D. G. Kwabi, Y. Ji, M. J. Aziz, *Chem. Rev.* **2020**, *120*, 6467; b) F. R. Brushett, M. J. Aziz, K. E. Rodby, *ACS Energy Lett.* **2020**, *5*, 879.
- [4] U. S. Schubert, O. Nolte, I. Volodin, C. Stolze, M. D. Hager, *Mater. Horiz.* **2021**, <https://doi.org/10.1039/d0mh01632b>.
- [5] a) M. Skyllas-Kazacos, M. Kazacos, *J. Power Sources* **2011**, *196*, 8822; b) L. Tong, Q. Chen, A. A. Wong, R. Gomez-Bombarelli, A. Aspuru-Guzik, R. G. Gordon, M. J. Aziz, *Phys. Chem. Chem. Phys.* **2017**, *19*, 31684; c) D. G. Kwabi, A. A. Wong, M. J. Aziz, *J. Electrochem. Soc.* **2018**, *165*, A1770.
- [6] S. Rudolph, U. Schröder, I. M. Bayanov, K. Blenke, D. Hage, *J. Electroanal. Chem.* **2013**, *694*, 17.
- [7] W. Duan, R. S. Vemuri, J. D. Milshtein, S. Laramie, R. D. Dmello, J. Huang, L. Zhang, D. Hu, M. Vijayakumar, W. Wang, J. Liu, R. M. Darling, L. Thompson, K. Smith, J. S. Moore, F. R. Brushett, X. Wei, *J. Mater. Chem. A* **2016**, *4*, 5448.
- [8] C. Stolze, M. D. Hager, U. S. Schubert, *J. Power Sources* **2019**, *423*, 60.
- [9] M. J. D. Low, R. T. Yang, *Spectrochim. Acta, Part A* **1973**, *29*, 1761.
- [10] S. W. Bruun, A. Kohler, I. Adt, G. D. Sockalingum, M. Manfait, H. Martens, *Appl. Spectrosc.* **2006**, *60*, 1029.
- [11] A. Gaigneaux, E. Goormaghtigh, *Analyst* **2013**, *138*, 4070.
- [12] a) T. Janoschka, N. Martin, M. D. Hager, U. S. Schubert, *Angew. Chem., Int. Ed.* **2016**, *55*, 14427; b) J. Luo, B. Hu, C. Debruler, T. L. Liu, *Angew. Chem., Int. Ed. Engl.* **2018**, *57*, 231; c) C. DeBruler, B. Hu, J. Moss, X. Liu, J. Luo, Y. Sun, T. L. Liu, *Chem* **2017**, *3*, 961.
- [13] G. Socrates, *Infrared and Raman Characteristic Group Frequencies: Tables and Charts*, John Wiley & Sons Inc, Hoboken, NJ **2004**.
- [14] S. Ressel, F. Bill, L. Holtz, N. Janshen, A. Chica, T. Flower, C. Weidlich, T. Struckmann, *J. Power Sources* **2018**, *378*, 776.
- [15] M. Pavelka, F. Wandschneider, P. Mazur, *J. Power Sources* **2015**, *293*, 400.
- [16] D. del Olmo, M. Pavelka, J. Kosek, *J. Non-Equilib. Thermodyn.* **2021**, *46*, 91.
- [17] W. Heller, *J. Phys. Chem.* **1965**, *69*, 1123.
- [18] a) J. Aldrich, *Int. Stat. Rev.* **1998**, *66*, 61; b) R. Geitner, T. Huang, S. Kupfer, S. Gräfe, F. Meirer, B. Weckhuysen, *Catal. Sci. Technol.* **2021**, *11*, 1626.
- [19] a) F. Despaigne, D. L. Massart, *Analyst* **1998**, *123*, 157R; b) J. Schmidhuber, *Neural Networks* **2015**, *61*, 85.
- [20] a) Y. Zhang, K. Ma, X. Kuang, L. Liu, Y. Sun, J. Xi, *J. Phys. Chem. C* **2018**, *122*, 28550; b) J. T. Vardner, A. A. Ye, D. A. Valdes, A. C. West, *J. Electrochem. Soc.* **2020**, *167*, 080512.